

# Collisional dynamics around binary black holes in galactic centers

Marc Hemsendorf<sup>1,3</sup>, Steinn Sigurdsson<sup>2</sup>, Rainer Spurzem<sup>3</sup>

## ABSTRACT

We follow the sinking of two massive black holes in a spherical stellar system. The massive particles become bound under the regime of dynamical friction. Once bound, the binary hardens by three body encounters with surrounding stars. Unlike other assumptions the massive system moves inside the core providing an enhanced supply of reaction partners for the hardening. These are the first results from simulations applying a hybrid “self consistent field” (SCF) and direct Aarseth  $N$ -body integrator (NBODY6), which synthesizes the advantages of the direct force calculation with the efficiency of the field method. The code is aimed for use on parallel architectures and is therefore applicable for collisional  $N$ -body integrations with extraordinarily large particle numbers ( $> 10^5$ ). It opens the perspective to simulate the dynamics of globular clusters with realistic collisional relaxation, as well as stellar systems surrounding a supermassive black hole in galactic nuclei.

## 1. Introduction

Collapse of baryonic matter in hierarchically clustering dark matter, and subsequent build-up of big galaxies from small ones via merging processes is nowadays the standard picture of galaxy formation and evolution (Peebles (1993), and for recent work e.g. Diaferio et al. (1999); Kauffmann et al. (1999a,b)). While the recent papers cited above can well reproduce the main global properties of galaxies and correlations, the details are still very much dependent on the gas physics and stellar feedback involved (cf. e.g. Navarro

---

<sup>1</sup>Department of Physics and Astronomy, Rutgers, the State University of New Jersey, 136 Frelinghuysen Road, Piscataway, NJ 08854-8019, USA  
e-mail: marchems@physics.rutgers.edu

<sup>2</sup>Department of Astronomy and Astrophysics, 525 Davey Lab, Penn State University, University Park, PA 16802, USA  
e-mail: steinn@astro.psu.edu

<sup>3</sup>Astronomisches Rechen-Institut, Mönchhofstr. 12-14, D-69120 Heidelberg, Germany  
e-mail: spurzem@ari.uni-heidelberg.de

and Steinmetz (2000)). On the other hand, most if not all galaxies harbor supermassive black holes in their center (Magorrian et al. 1998; Richstone et al. 1998; Kormendy and Richstone 1995). Correlations have been detected recently between the black hole mass and the galaxy’s mass and central velocity dispersions (Ferrarese and Merritt 2000; Gebhardt et al. 2000). This is strong evidence that the central black holes in galactic nuclei are linked to the history of the galaxy itself. Haehnelt and Kauffmann (2000) and Kauffmann and Haehnelt (2000) demonstrate how this is consistent with the framework of semi-analytic models that follow the formation and evolution of galaxies in a cold dark matter-dominated universe. They assume supermassive black holes are formed and fueled during major mergers, and so explain qualitatively many aspects of the observed evolution of galaxies, including the observed relation between bulge luminosity and velocity dispersion and black hole mass. As already discussed by (Begelman et al. 1980) such picture requires the formation of galactic nuclei containing more than one black hole, maybe even more, depending on the black hole merger rate relative to the galaxy merger rate. Observationally, there is, however, very little evidence for massive black hole binaries (Lehto and Valtonen 1996; Halpern and Eracleous 2000). That has led Gould and Rix (2000) to propose alternative mechanisms to the minimal stellar dynamical processes, which can lead to a rapid decay of massive black holes into the center of a galaxy and the subsequent merger of black holes Gould and Rix (2000). Note, that Begelman et al. (1980) had already proposed that gas infall may in some circumstances dominate in the critical phase to orbital evolution of a black hole binary, to overcome a gap in time scales prohibiting the final merger.

On the other hand, if there is no way to a quick merger, these nuclei would be freed from the black hole multiples through slingshot ejections (Valtonen et al. 1994). As will be discussed later, dynamical friction following Chandrasekhar (1943) is not sufficiently effective in order to lead to a rapid coalescence of a black hole binary. Once the binary system becomes hard, the high orbital velocity of the massive objects allows only further hardening through close encounters and three body interactions with stars. Such processes will evacuate the field stars from the surrounding of the massive bodies, so it can be argued that the stellar scatterings do not suffice for rapid coalescence. Here it is assumed that the center of mass of the binary does not move with respect to the stellar system. We show that even with a fairly symmetrical initial setup the binary gains some linear momentum. This introduces a wandering motion which exceeds the expectations from equipartition. By this the stellar supply for the binary hardening is guaranteed and rapid coalescence through purely stellar dynamical processes possible. Our new method allows us to study in detail three-body interactions of a black hole binary with field stars. Although the perturbing mass of the field stars is small compared to the black hole mass, there are very many stars, and each encounter can lead to changes in binding energy and eccentricity of the black hole

binary. As we see in our models, the black hole binary keeps a rather high eccentricity due to the encounters. High eccentricity will very efficiently speed up gravitational radiation mergers, and are, as noted by Gould and Rix (2000), a way to produce massive black hole mergers in a purely stellar dynamical way.

The correct theoretical prediction of the frequency of black hole mergers in galactic environments will be important for the search for gravitational waves. The merging of supermassive black holes of  $3 \cdot 10^4$  to  $3 \cdot 10^7 M_\odot$  in the nuclei of merging galaxies and protogalaxies can be heard with high signal to noise at redshifts from 0 to 100 (Phinney 2000) by the Laser Interferometer Space Antenna (LISA, Danzmann (2000))

Previous attempts to tackle this situation have been done either by solving the perturbed two and three body problem in simplified models (Mikkola and Valtonen 1992) or by direct  $N$ -body models. Since the mass differences between the massive bodies and the stellar bodies is so large, high particle numbers are required in order to model the relaxation processes around the black holes accurately. The simulations so far used softened particles on special purpose computers (Makino et al. 1993; Makino 1997) or a hierarchical hybrid code in which only all forces involving the black hole particles are Newtonian (Merritt and Quinlan 1998; Quinlan and Hernquist 1997). This allows to boost the particle numbers to orders of  $10^4$ . As this shows, the modeling of binary black hole hardening turns out to be extremely challenging, algorithmically and computationally. In this paper we are describing a new hybrid field-particle code, which treats all those particles, whose orbit is leading them to the central regions of the system, with a high precision direct  $N$ -body method appropriate for collisional stellar dynamics. In order to adapt both parts of the hybrid code to each other, the field method (approximating the potential exerted by a set of particles by a series expansion, often known as “SCF”) had to be upgraded to a fourth order Hermite integrator using also the time derivative of the potential, as in the modern direct  $N$ -body codes. This new code is then applied to the binary black hole problem.

In the following some details of the sinking black hole problem are introduced. Section 3 introduces the integration software used for the numerical experiments described in this paper. Section 4 is devoted to a comparison between the new collisional code *EuroStar* with a well used workhorse in this field called *NBODY6* (Aarseth 1993, 1996, 1999), using its parallel implementation *NBODY6++* (Spurzem and Baumgardt 2001; Spurzem 1999). The application of the code to the sinking binary black hole problem is reported in section 5.

## 2. The sinking binary black hole problem

Following Begelman et al. (1980), the central black holes of two galaxies will coalesce in the course of a galactic merger. During the early stages of the merger, the stellar component will form a nearly spherical system within the short timescale for violent relaxation. After that, the two supermassive black holes move through the stellar component with a velocity similar to the initial relative motion between the two galaxies. From this moment on, both massive bodies will feel dynamical friction. This friction leads the black holes to the newly-formed galactic center, while the frictional force becomes more efficient with increasing density. Through this process, the black holes must inevitably ‘find’ each other and form a binary system (Makino 1997).

After being bound, the binary hardens through dynamical friction. Assuming the center of mass of the binary to be fixed at the center of mass of the surrounding galaxy, dynamical friction must become less efficient with increasing binding energy of the binary. An encounter on a timescale longer than the orbital timescale of the binary cannot harden it efficiently. Close encounters and three body interactions become more and more efficient for the hardening process. The most efficient process for binary hardening in this stage are the stars which gain very large velocities in three body encounters with the black holes. Because this process can evacuate the surrounding of the binary from stars, the hardening timescale can become very long. However, this is not true if the supply of stars undergoing close three body encounters with the supermassive objects remains high. N-body simulations with high particle numbers can help set constraints on this problem (Makino et al. 1993; Quinlan and Hernquist 1997).

## 3. Collisional stellar dynamics with EuroStar

A numerical simulation of the hardening phase (until the massive black holes start to send out gravitational waves) must be able to follow three body encounters. For this reason, the Keplerian potential should not be softened in the dense part of the integrated system. The code must be able to integrate large angle encounters in an efficient way, while neither requiring too much computing time nor introducing energy errors. The overall N-body integration does not need to be symplectic, but should keep the energy error as low as possible. On the other hand, in a system showing a core halo structure the bulk of the stars in the halo move in the regime of the mean field of the whole cluster. Computationally, the central part of the system could best be treated using a collisional integrator, the halo part of the central galactic cluster by a mean field method.

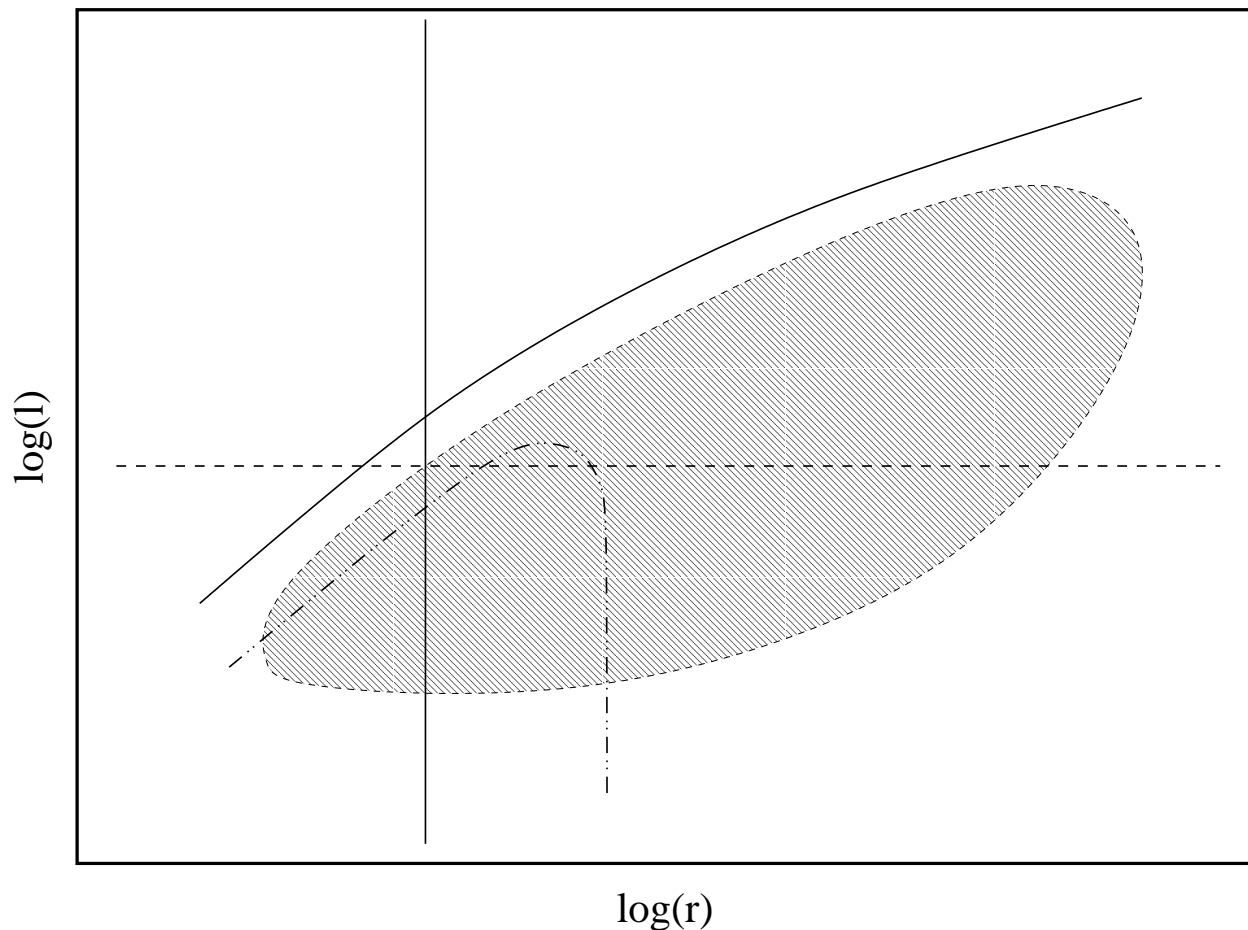


Fig. 1.— Schematic decomposition of a star cluster according to its angular momentum distribution. The hatched region symbolizes the distribution of angular momentum per unit mass as a function of radius. The solid curve above shows the angular momentum of particles on circular orbits with escape velocity. As such, it functions here as an upper bound for the angular momentum at a given radius, or as a lower limit for the radius a star can reach with fixed angular momentum. If the cluster is divided into two parts by a critical value for  $l$ , as shown by the horizontal dashed line, halo particles which never reach the core can be distinguished from particles which can move deep in to the core (vertical solid line). The dot-dot-dashed line shows the maximal angular momentum for a set of particles selected by an energy criterion. Such a selection would not affect all particles below that line. In fact, an energy criterion is not sufficient for selecting all collisional particles in our system.

In the new method EuroStar, both the collisional code NBODY6++ (Aarseth 1993, 1999; Spurzem and Baumgardt 2001) and the collisionless method using series expansion to approximate the potential (generally known and referred to as “SCF” (Hernquist and Ostriker 1992; Hernquist et al. 1995; Zhao 1996; Sigurdsson et al. 1997; Holley-Bockelmann et al. 2001), which we use henceforth as an abbreviation here as well) are merged to optimize large- $N$  collisional  $N$ -body simulations: The cluster, which is assumed to be in equilibrium, is divided into two sections, applying a critical angular momentum criterion. As shown in figure 1, it is hereby possible, to distinguish between particles orbiting solely in the halo from the ones which have trajectories leading through the core of the system.

In a stationary gravitational point mass system, two-body relaxation leads to an exchange between halo particles and core particles in such a divided cluster. For particle numbers above  $10^4$  only a very small number of particles cross the border per dynamical time. This is very fortunate in the sense that it allows us to integrate the orbits of the halo particles with a collisionless method and the core particles with a collisional code. An exchange of particles would cause energy conservation problems since the contribution of a particle to the main potential would be changed from Keplerian to a sample point of a mean field in *EuroStar*.

NBODY6++ does the integration of the point masses in the core of the system. It is an Aarseth type direct force integrator applying the Hermite integration scheme. NBODY6++ gains its efficiency by implementing an Ahmad-Cohen neighbor scheme and individual block time-steps (Ahmad and Cohen 1973; Aarseth 1999). Close interactions between particles are treated by regularization of the equations of motions (Kustaanheimo and Stiefel 1965). NBODY6++ scales very well parallel architectures and is also usable with the special purpose computer GRAPE (Spurzem and Kugel 1999; Sugimoto et al. 1995). The Hermite scheme requires one to compute  $\mathbf{F}_i$  and  $\dot{\mathbf{F}}_i$  on each time-step but allows one to approximate the particle’s orbit to fourth order. This is done by interpolating the higher derivatives through a predictor corrector scheme (Aarseth 1996).

$$\mathbf{F}_i = - \sum_{j \neq i} \frac{Gm_j \mathbf{r}_{ij}}{r_{ij}^3}, \quad (1)$$

$$\dot{\mathbf{F}}_i = - \sum_{j \neq i} Gm_j \left[ \frac{\mathbf{v}_{ij}}{r_{ij}^3} + \frac{3(\mathbf{v}_{ij} \cdot \mathbf{r}_{ij}) \mathbf{r}_{ij}}{r_{ij}^5} \right]. \quad (2)$$

The SCF method qualifies for the collisionless part of the system since the basis functions are given analytically. This allows one to implement the Hermite scheme for SCF, which makes SCF an ideal far force extension to NBODY6++. Its drawback however is that this method restricts the input systems to have approximately a spherical particle distribution

around the coordinate center, the possible deviation depends on the number of spherical harmonics used for the expansion. In order to have better convergence, one parameter basis functions for  $\rho_{nlm}(\mathbf{r})$  and  $\Phi_{nlm}(\mathbf{r})$  come into use as follows Zhao (1996):

$$\rho_{nlm}(\mathbf{r}) = \sqrt{4\pi} \frac{K_{nl} r^l C_n^{(\omega)}(\xi)}{r^{(2-\frac{1}{\alpha})} (1 + r^{\frac{1}{\alpha}})^{2+\alpha(2l+1)}} Y_{lm}(\vartheta, \varphi), \quad (3)$$

$$\Phi_{nlm}(\mathbf{r}) = - \frac{\sqrt{4\pi} r^l C_n^{(\omega)}(\xi)}{(1 + r^{\frac{1}{\alpha}})^{\alpha(2l+1)}} Y_{lm}(\vartheta, \varphi). \quad (4)$$

The  $C_n^{(\omega)}$  are called ultraspherical or Gegenbauer polynomials. The spherical harmonics are given by the  $Y_{lm}(\vartheta, \varphi)$ . Once the  $A_{nlm}$  for a certain set of particles are known, an analytic expression of the potential and the density is found. Due to the truncation of the expansion they represent the mean field and mean density. This means that the force at each position and its derivative can be computed using the following expressions:

$$F(\mathbf{r}) = - \sum_{nlm} A_{nlm} \nabla \Phi_{nlm}(\mathbf{r}), \quad (5)$$

$$\dot{F}(\mathbf{r}) = - \frac{d}{dt} \left( \sum_{nlm} A_{nlm} \nabla \Phi_{nlm}(\mathbf{r}) \right). \quad (6)$$

Since this is a significant modification of the SCF scheme which leads to equations (5) and (6), we are providing them in a more detailed form in the Appendix.

#### 4. Testing the hybrid code

One of the first scientific applications for the new method is to follow the last stages of an ongoing merger between two galaxies containing a supermassive black hole. First the results from EuroStar were checked against the results from a fully collisional run using NBODY6++. As an initial setup it is assumed that the stellar systems have already arranged themselves into a spherical system. The two formerly central supermassive black holes are moving through the stellar component with a speed on the order of the orbital velocity of the two initial galaxies.

In the present simulations, the stellar component is a realization of a Plummer model with the Plummer radius  $R = 3\pi/16$ . The half mass radius of this system is at a radius of  $r_h \approx 0.78$  in the model units of the simulations. The total mass of the system is unity. The gravitational constant is set to unity as well, conforming to the model units described by Heggie & Mathieu (1986).

The particles, for modeling the black holes, contain 1% of the total system’s mass. Their initial position is at  $x = \pm 0.5$ , and their initial velocity is 13.6% of the circular velocity at their initial radius.

The orbits of black holes during the simulation are analyzed by means of the classical two-body problem. The binding energy and the eccentricity of the black hole orbit is computed from their distance and relative velocity, assuming a Keplerian potential. Once the black holes become bound, their two-body attraction will be the most important force for each other. The eccentricity of the binary  $\epsilon$  and the binding energy  $h$  are computed as follows, using the definition  $\mathbf{r} = \mathbf{r}_a - \mathbf{r}_b$ . The vectors  $\mathbf{r}_a$  and  $\mathbf{r}_b$  denote the position vectors of the massive particles  $a$  and  $b$ . From this it follows that (Boccaletti and Pucacco 1996):

$$h = \frac{1}{2} m_{\text{red}} \dot{r}^2 + \frac{|\mathbf{l}|^2}{2 m_{\text{red}} |\mathbf{r}|^2} - \frac{m_a m_b}{|\mathbf{r}|}, \quad (7)$$

$$a = - \frac{m_a m_b}{2 h}, \quad (8)$$

$$\epsilon = \sqrt{1 + \frac{2 h |\mathbf{l}|^2}{m_{\text{red}} (m_a m_b)^2}}, \quad (9)$$

with  $\mathbf{v} = \dot{\mathbf{r}}$  and

$$\dot{r} = \frac{1}{|\mathbf{r}|} \mathbf{v} \cdot \mathbf{r}, \quad (10)$$

$$m_{\text{red}} = \frac{m_a m_b}{m_a + m_b}, \quad (11)$$

$$\mathbf{l} = m_{\text{red}} \mathbf{r} \times \mathbf{v}. \quad (12)$$

This method of analysis provides a sensitive measure for the moment, when the black holes become bound to each other. Furthermore, this way of analyzing the data also offers a precise tool to follow the hardening of the binary.

Since this sinking binary problem is the first application for the new hybrid method EuroStar, the results from the new method are compared with the ones from the fully collisional code NBODY6++, for smaller total particle numbers. Last but not least, the problem is simulated by the hybrid code using 65536 particles. Figure 2 shows the result for two comparative runs, using 16384 particles. The plot on the left hand side in figure 2 shows the numerical eccentricity of the binary as a function of the simulated time in model units. The plot on the right hand side shows the two-body binding energy as a function of time. The binary becomes bound after 10 time units, in both cases.

The fully collisional method and the hybrid code EuroStar show slightly different sinking rates for the binary at the beginning of the simulation. These differences result from the



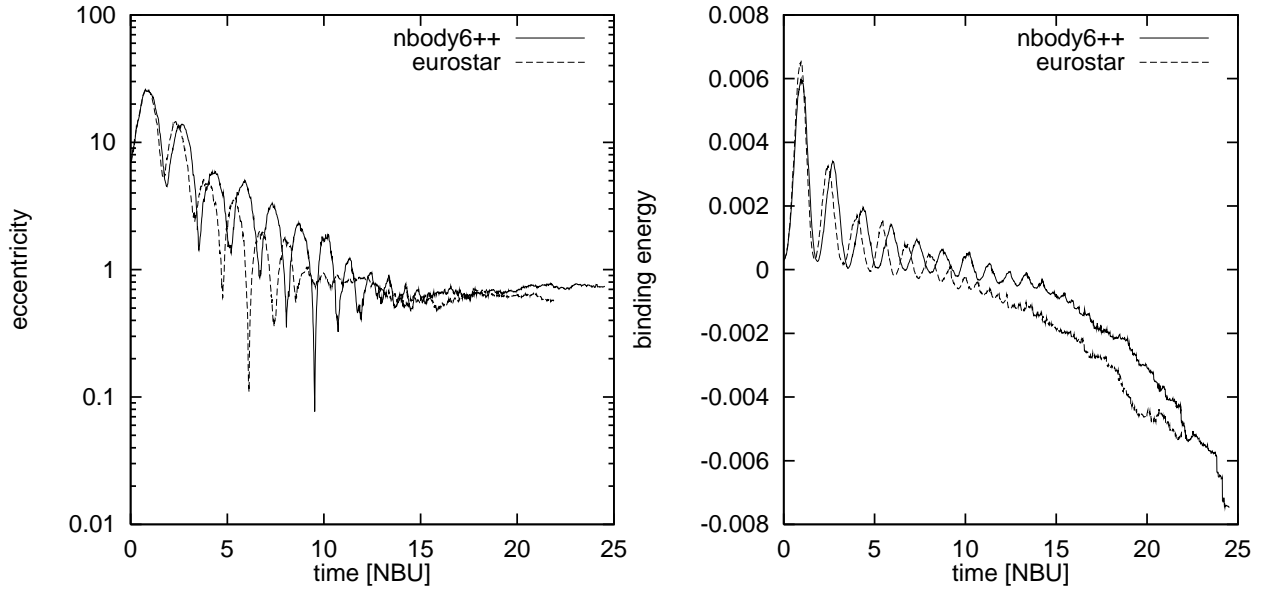


Fig. 2.— Development of the orbit eccentricity of the black hole binary as a function of time in model time units (left) and its binding energy as a function of time. The results for the direct method are shown by the solid line (NBODY6++), the ones for the hybrid code (EuroStar) are given by the dashed line. Note, that if the binary is not yet bound, equations (8) and (9) formally yield values of  $a > 0$  and  $e > 1$ . This means that in that phase the black holes are still not yet gravitationally bound to each other.

different density of collisional particles around the black holes in both codes. While the black holes in the fully collisional run suffer small angle encounters with every particle in the system, this is naturally not possible in the hybrid code. In this case, all particles treated by the mean field method can only interact with the system through changes in the mean potential. After the binary has become bound, the hardening process is driven by the stars which have a small enough impact parameter, such that they have an encounter timescale smaller than the orbital timescale of the massive binary. Therefore the hardening depends more on the neighboring particles, which have large orbital velocities.

With increasing simulation time, the binary locks into an oscillating motion around the center of mass of the stellar component. Nevertheless this motion does not reach outside of the dense galactic core. Effectively the differences in the density of the collisional particles between the two methods vanish, after the binary has become bound. Figure 2 reflects this by showing a parallel evolution of eccentricity and binding energy for times larger than 10 time-units in the simulation.

## 5. Hardening of a massive binary

### 5.1. Initial conditions

The particles representing the stellar component are distributed according to Plummer’s model with  $R = 3\pi/16$ . The total mass of the stars is fixed to 0.98, while the massive particles carry 0.01 each, so  $M_{\text{tot}} = 1.0$ . The massive particles are initially placed symmetrically around the center of mass of the stellar component. Their initial radius is at  $r \approx 0.64r_h$ , their initial velocity is 13,6% of the circular velocity at this radius. In the given model units this represents a starting point for the black holes at  $x = \pm 0.5$  and  $v_y = \pm 0.1$ . The center of mass of the stellar component is at the origin. The mass factor between a stellar particle and a black hole particle is 1338.5 for 131072, 669.7 for 65536, and 335.4 for 32768 particles.

In order to have a small statistical basis for analysis, we compare the results from five runs with 32768 particles, two runs with 65536 particles, and three runs with 131072 particles. Not all runs reached the 60 time units mark due to time step scheduling problems caused by accuracy problems in very close encounters between stars and a massive particle. However, until then, the simulations conserved the total energy with relative errors below  $10^{-4}$ . In all runs the binary becomes bound at approximately 10 time units.

The parameters of the hybrid code have been adjusted in the following way: The SCF part uses the parameter  $\alpha = 0.5$  for the basis functions. By this, the basis functions represent a Plummer model in zeroth order, which is in accordance with the models used by Clutton-

Brock (1973). Also, this choice ensures an optimal representation of the actual potential by the expansion method. To allow flexibility in the expansion, seven basis functions came to use for the radial direction and five ( $l = [0..5]$ ,  $m = [-5..5]$ ) for the angular expansions. The NBODY part uses an  $\eta_i = 0.01$  for the irregular time-steps and an  $\eta_r = 0.02$  for the regular time-steps. Furthermore, the Ahmad-Cohen neighbor scheme (Ahmad and Cohen 1973) has been modified in such a way that the search radius for neighbors is enhanced by a factor of 7.7, 14.4, and 27.7 for the runs with 32768, 65536, and 131072 particles respectively.

## 5.2. The motion of the massive bodies

In order to compare the runs, all data have been binned for the parameter  $t$ , which represents the integrated time of the system in  $N$ -body time units (Heggie and Mathieu 1986). Table 1 gives the number of sample points for the orbital data on the massive particles. For technical reasons, the runs with 131072 particles could not be continued until they reach 60 time units. When we are binning the total particle number  $N_{\text{tot}}$ , table 1 shows the number of samples in the row labeled “total”. In the following, we present the results for the motion of the massive binary within the stellar system.

Figure 3 shows the evolution of the quantity  $\langle 1/a \rangle$  as the average from the runs above. Equation 8 serves to compute the semi-major axis  $a$  from the orbital data of the runs. According to the prescription above the data is binned for comparison. From the data in each bin we evaluate the average  $\langle 1/a \rangle$  and the standard deviation. In order to find the hardening rate, we fit the averages, plotted as circles in figure 3, with a line. The standard deviation of the data, given in the plot as the error-bars, serves for the weighing factors.

For the average over all runs as plotted in figure 3 the regression line has a inclination of  $8.7 \pm 0.4$ . Depending on the number of particles the inclination is  $9.6 \pm 0.5$  for 32768,  $8.6 \pm 0.2$  for 65536, and  $6.8 \pm 0.2$  for 131072 particles, which suggests a dependency of the particle number in the results. Compared with other quantities the noise level in the data for  $1/a$  is low. For the bins at  $t = 52.5$  and  $t = 57.5$  the input data from the runs with 32768 particles shows strong steplike changes of  $1/a$  to higher and lower levels resulting from three body interactions with surrounding stars. This is due to the small particle number.

In order to study the evolution of the angular momentum of the bound binary we plot angle  $\theta$  between the  $z$ -coordinate axis and  $1/l$  as shown in figure 4. Initially  $\theta$  is vanishing. As with  $\langle 1/a \rangle$  all data from the simulations is binned and averaged. The open circles in figure 4 represent the average and the error bars the standard deviation in the data.

Once the binary becomes bound, the values for  $\theta$  change only slightly in all simulations.

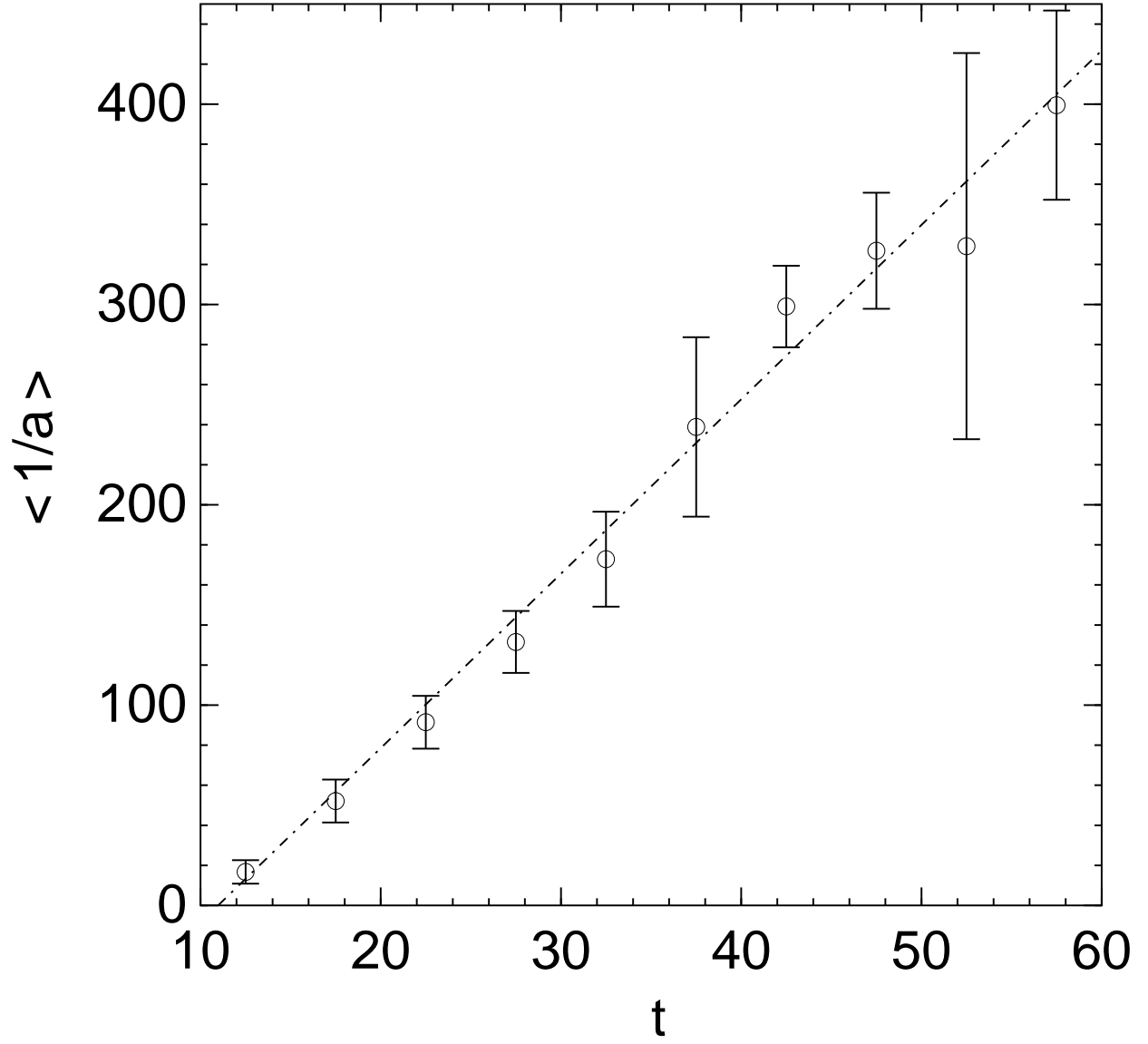


Fig. 3.— Evolution of  $\langle 1/a \rangle$  as a function of time, after the binary becomes bound. The averages have been taken over all runs carried out. The error-bars are showing the standard deviation of the data in the bins.

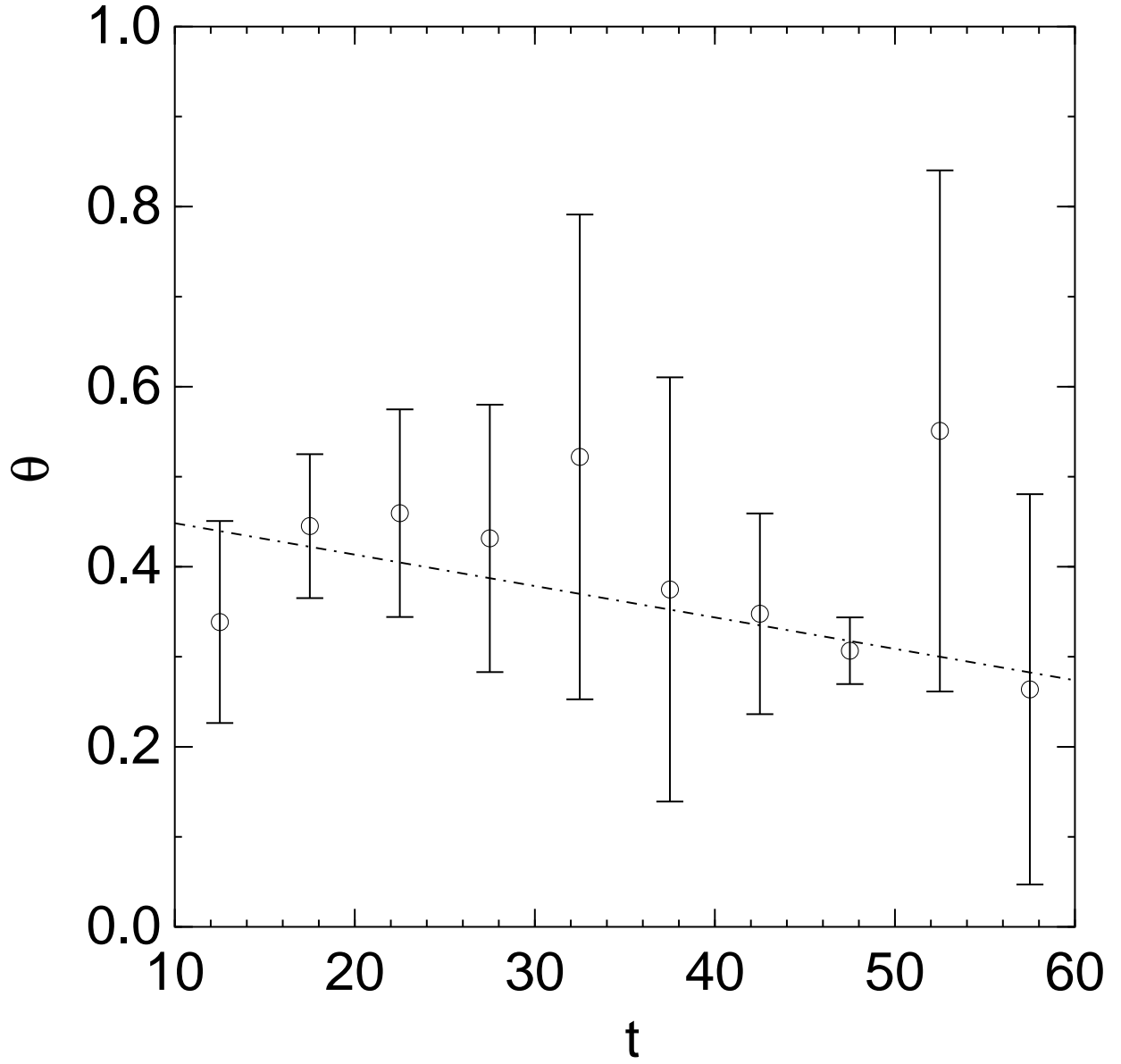


Fig. 4.— Evolution of polar angle  $\theta$  of the angular momentum of the massive binary after it has become bound. The angular momentum vector is aligned to the  $z$ -axis initially.

Averaged over the time span between the first bound orbit of the massive particles and the end of the simulations, the value for average of  $\theta$  becomes  $0.5 \pm 0.3$  for he runs with 32768,  $0.3 \pm 0.1$  for 65536, and  $0.5 \pm 0.1$  for 131072 particles.

Taking the average over all runs and binning the time, as shown in figure 4, the results can be fitted by a straight line. The inclination of this line is  $-0.003 \pm 0.003$ . When we group the simulations according to their particle number, the fitting lines have an inclination of  $0.016 \pm 0.004$  for he runs with 32768,  $-0.0044 \pm 0.0006$  for 65536, and  $0.006 \pm 0.002$  for 131072 particles. Though being small, these inclinations are all significantly nonzero and distinct from each other. Torque forces are acting on the binary system through the simulations. Especially the data for the runs with the small particle number and the small mass ratio between a black hole and a stellar particle is very noisy and shows steplike changes of  $\theta$ .

While  $\theta$  evolves in an ordered way until the binary becomes bound, the angle between the  $x$ -coordinate axis and the normalized angular momentum vector,  $\phi$  behaves more randomly. Until the massive particles become bound  $\phi$  changes rapidly reaching all values between 0 and  $2\pi$ . Once the binary becomes bound,  $\phi$  settles at an individual value for each run. The evolution from there on is in same order of magnitude as for  $\theta$ .

By studying the wandering of the binary using the quantity  $\langle r_{\text{com}}^2 \rangle$  as a function of the total particle number we can compare the found motion to the expected Brownian motion in the system.  $r_{\text{com}}$  is the distance of the center of mass of the black holes from the center of mass of the stellar system. Figure 5 implies that the mean motion is not constant with time. However, the inclination of the fitting line is  $(1.0 \pm 1.1) \cdot 10^{-5}$  which means the behavior could be also constant within  $1\sigma$  uncertainty. For the individual particle number groups the situation is as follows: For 32768 particles we find  $(0.6 \pm 1.5) \cdot 10^{-5}$ , for 65536 particles  $(1.0 \pm 0.7) \cdot 10^{-5}$ , and for 131072 particles  $(0.9 \pm 7.8) \cdot 10^{-6}$ .

Compared to its mean value over the whole simulation, the evolution of  $\langle r_{\text{com}}^2 \rangle$  with time introduces change of not more than 10%. For this reason, we assume  $\langle r_{\text{com}}^2 \rangle$  to be constant for the analysis of the Brownian motion as a function of the particle number.

Figure 6 shows the mean squared distance between the center of mass of the massive system and the stellar system as a function of the total particle number of the simulations. The inclination of the fitting line is  $(-4.5 \pm 5.6) \cdot 10^{-9}$ . Given our small sample of runs we can not determine a dependency of  $\langle r_{\text{com}}^2 \rangle$  on the particle number.

The figures 7 and 8 show the evolution of  $\langle v_{\text{com}}^2 \rangle$  as a function of time and total particle number  $N_{\text{tot}}$ . The quantity  $v_{\text{com}}$  is the velocity of the center of mass of the black holes relative to the velocity of the center of mass of the stellar system. As before, we are comparing its behavior as a function of time and total particle number.

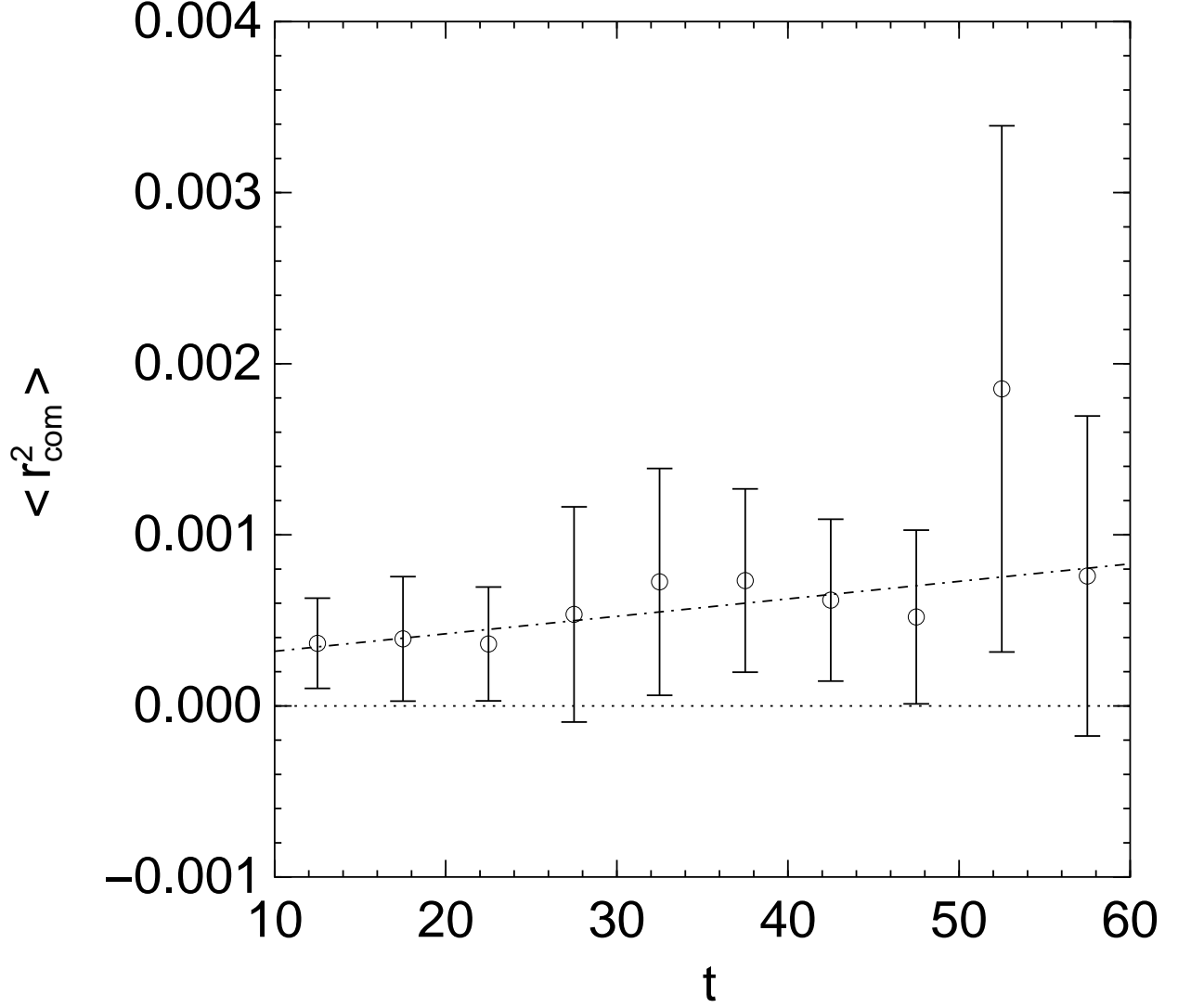


Fig. 5.— The mean of  $r_{\text{com}}^2$  taken over the all simulations as a function of the integrated time in  $N$ -body units. The quantity  $r_{\text{com}}$  is the distance of the center of mass of the black hole binary to the center of mass of the stellar particles.

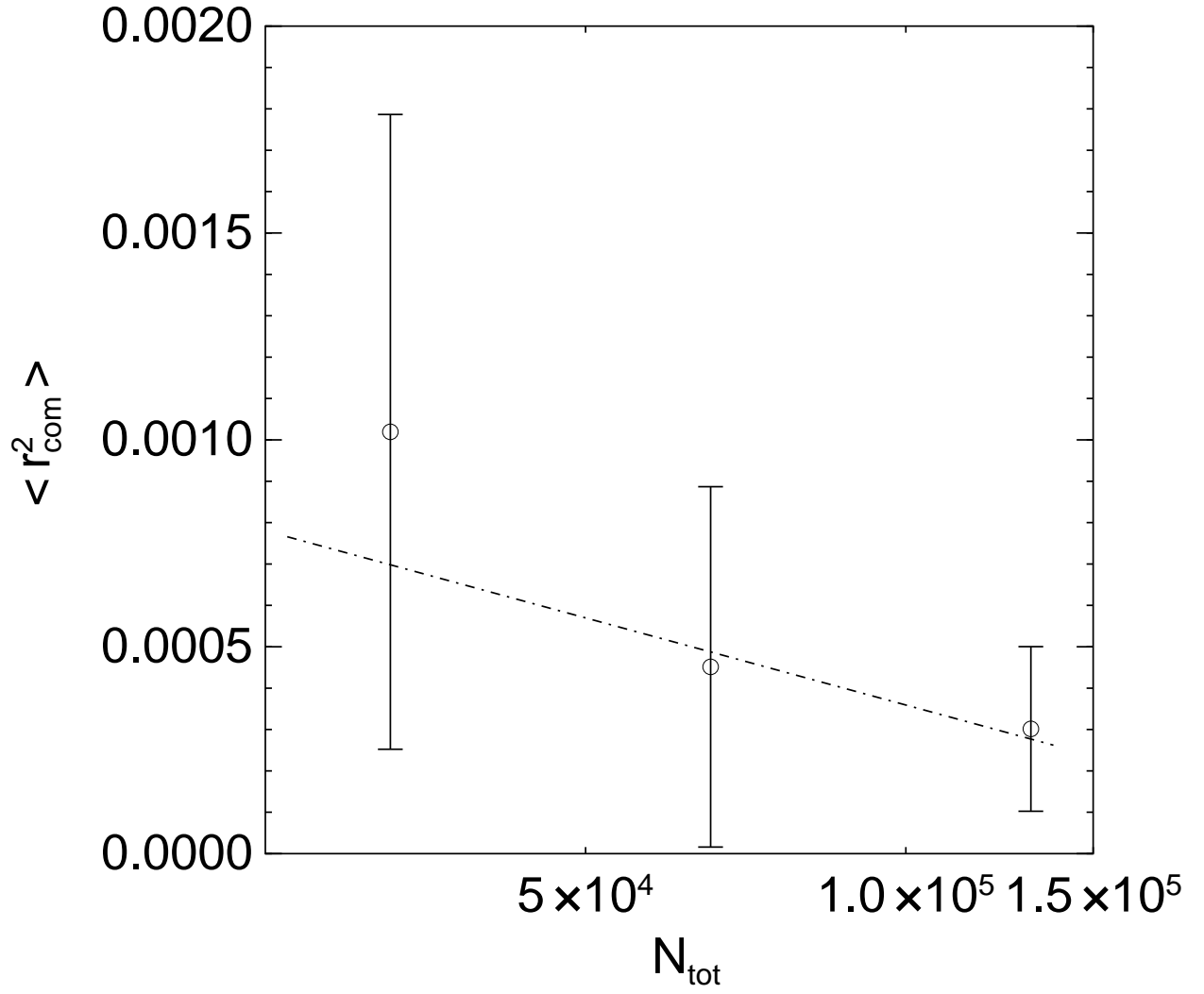


Fig. 6.— The mean of  $r_{\text{com}}^2$  taken over the full integrated times as a function of the total number of particles in the simulations. The quantity  $r_{\text{com}}$  is defined as in figure 5.



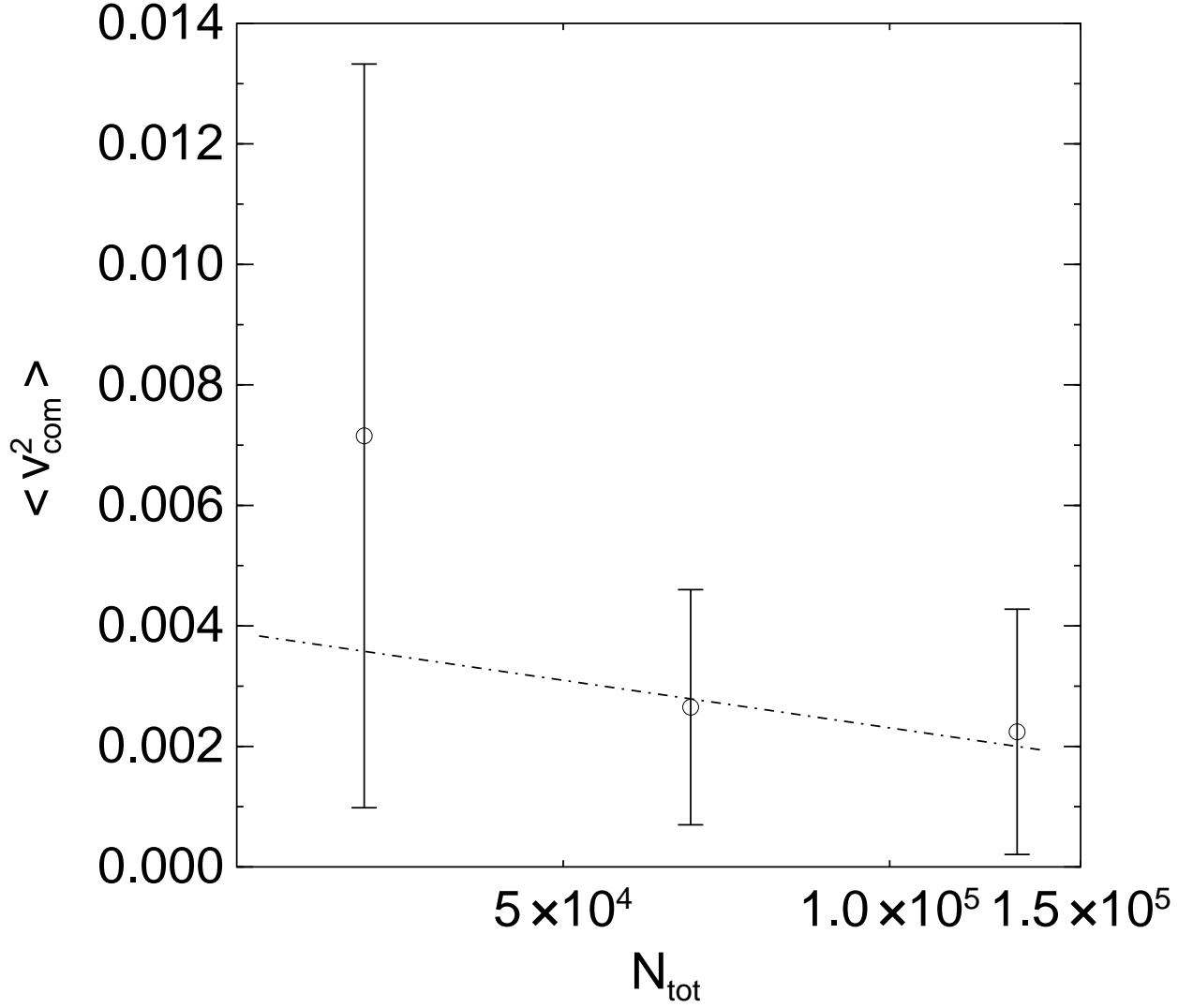


Fig. 7.— The mean of  $v_{\text{com}}^2$  as a function of the total particle numbers in the simulations. The values for  $v_{\text{com}}^2$  have been averaged over the total simulation time, the error-bars represent the standard deviation in the data.  $v_{\text{com}}$  is the relative motion of the center of mass of the massive binary relative to the center of mass of the stellar system.

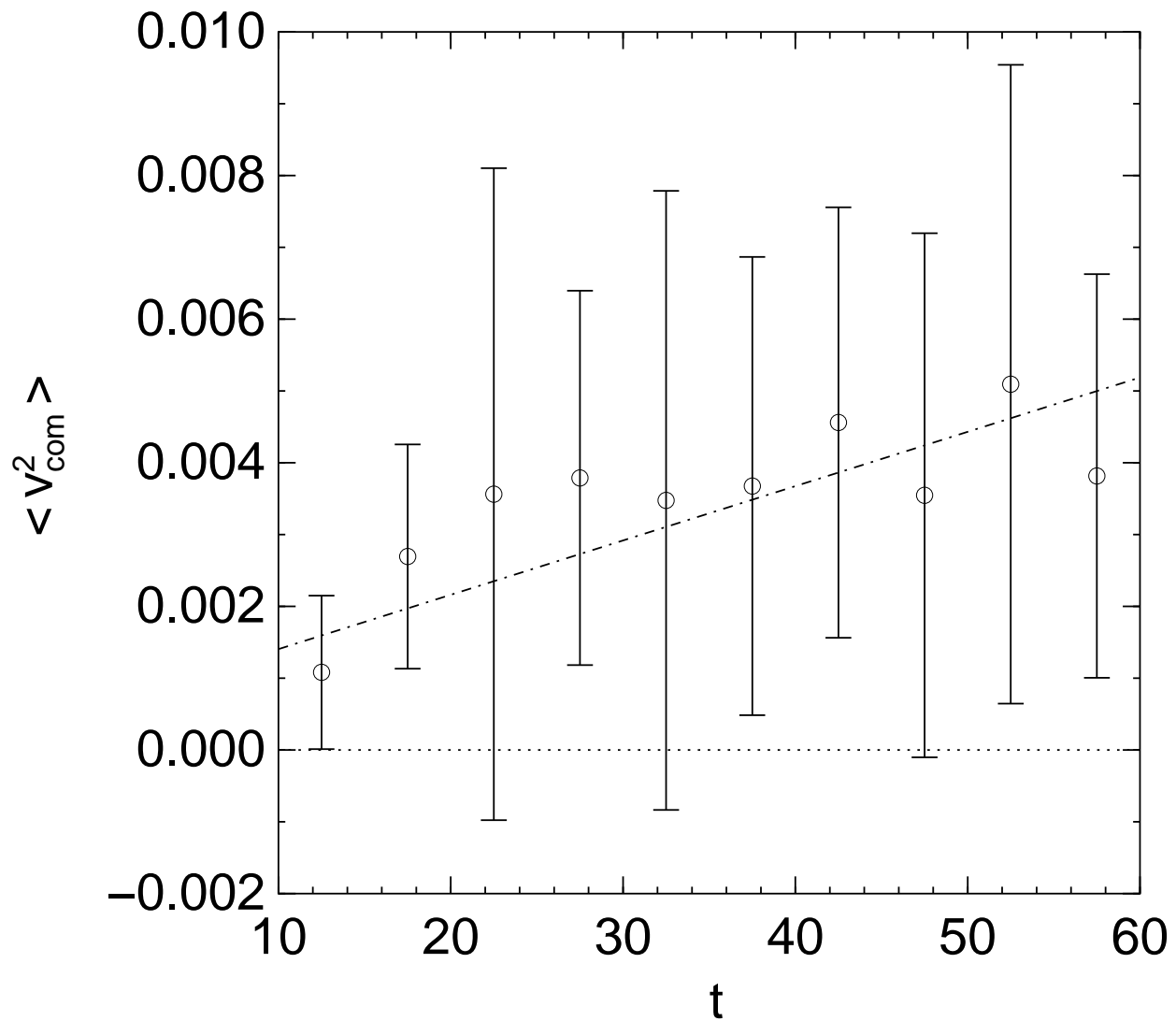


Fig. 8.— The mean of  $v_{\text{com}}^2$  as a function of the integrated time in  $N$ -body units. The values for  $v_{\text{com}}^2$  have been averaged of the bins in time, the error-bars represent the standard deviation in the data.

We find an inclination of  $(7.6 \pm 4.9) \cdot 10^{-5}$  for the fitting line in figure 8. Depending on the total particle number, this inclination is  $(3.5 \pm 7.0) \cdot 10^{-5}$  for 32768,  $(2.6 \pm 2.4) \cdot 10^{-5}$  for 65536, and  $(4.2 \pm 4.0) \cdot 10^{-5}$  for 131072 particles. The inclination for the line in figure 7 is  $(-1.7 \pm 3.9) \cdot 10^{-8}$ .

In order to study the influence of dynamical friction on the decay of the binary orbit we analyze the behavior of its orbital angular momentum as a function of time. As figure 9 shows, the decay shows a two mode evolution. Between 0 and 20 time-units linear regression for  $\langle \lg(l) \rangle$  gives a slope of  $(-6.8 \pm 0.9) \cdot 10^{-2}$ . The line with the more shallow slope represents the behavior between 20 and 60 time-units. Its slope is  $(-1.3 \pm 0.2) \cdot 10^{-2}$ .

### 5.3. Reaction of the stellar system

The stellar system reacts to the motion of the black hole in a generic fashion. We find that our statistical basis is too small for finding a clear dependency of the results from the total number of particles in the simulations. For this reason we are only presenting the averages from all of our runs.

Figures 10 and 11 show the evolution of the density and the velocity dispersion for particles with a radius of 0.032 or smaller averaged over our runs as a function of time. While the black hole binary becomes bound at  $\approx 10$  time-units the density has a maximum at  $\approx 18$  time-units. The velocity dispersion is highest at  $\approx 23$  time-units.

A linear fit ( $y = a + bx$ ) can be applied to the evolution of  $\rho$  and  $\sigma$  between 20 and 60 time-units as plotted in figures 10 and 11. For  $\langle \rho \rangle$  we find  $a = 2.6 \pm 0.7$  and  $b = -0.028 \pm 0.016$ , for  $\langle \sigma \rangle$  we find  $a = 2.8 \pm 0.6$  and  $b = -0.030 \pm 0.013$ .

## 6. Discussion

### 6.1. Hardening rate

Following Hills (1992), and Quinlan (1996) the hardening rate of a massive binary floating in a sea of light stars is given by:

$$\frac{d}{dt} \frac{1}{a} = H \frac{G\rho}{\sigma}. \quad (13)$$

With  $G = 1$  and the assumption that the average for  $\rho$  and  $\sigma$  evolves in the same way between 20 and 60 time-units, we find  $H = 8.7 \pm 0.4$ . This value is significant smaller than the ones given by Hills (1992)  $H_{\text{Hills}} = 13.5$  and Quinlan (1996)  $H_{\text{Quinlan}} \approx 18$ .

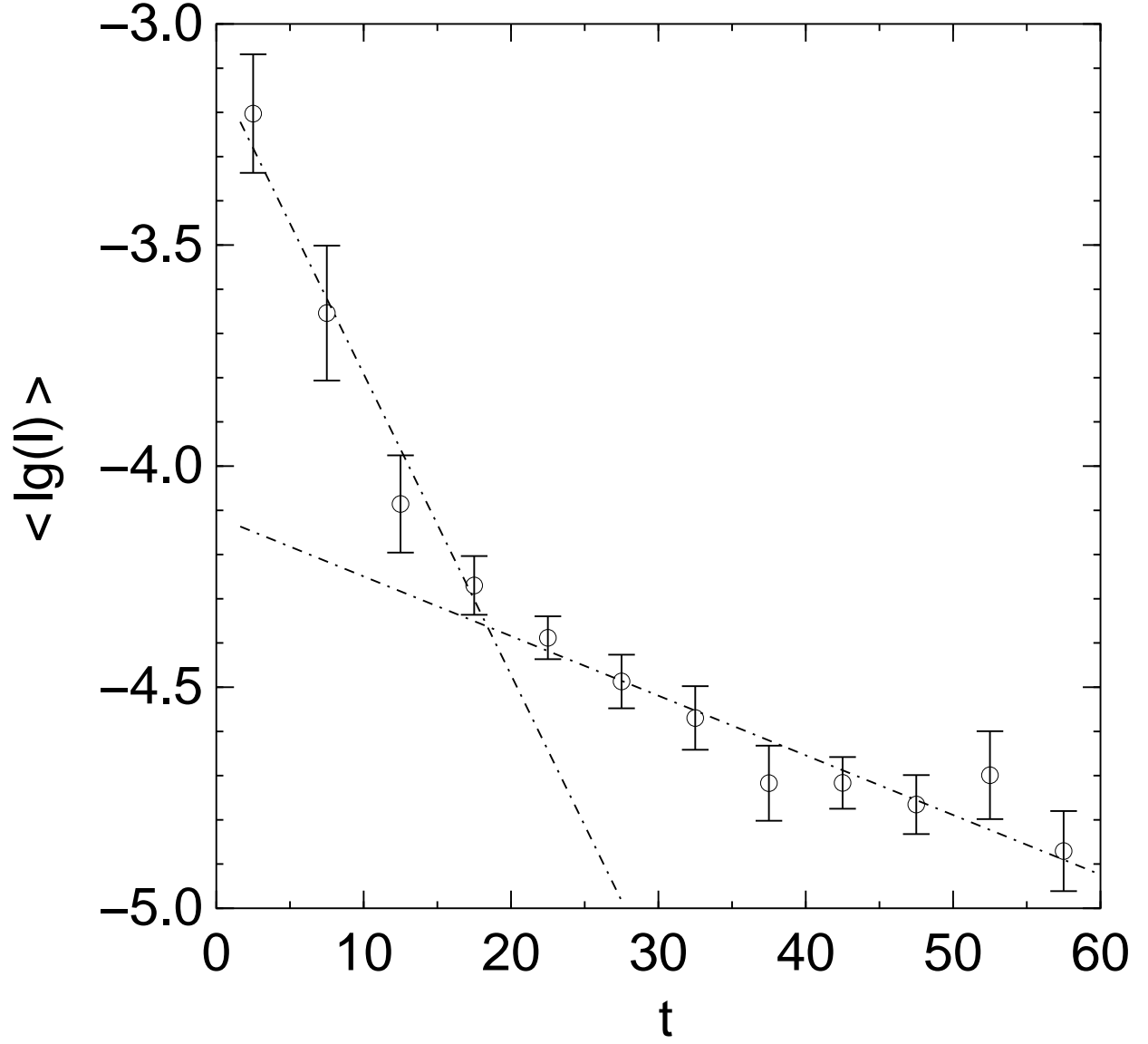


Fig. 9.— The evolution of the orbital angular momentum as a function of time for the collected data of the runs. The error bars represent the standard deviation in the data. In order to distinguish between the two modes of the evolution, linear regression is applied to the bins between 0 and 20 and 20 and 60 time-units separately.

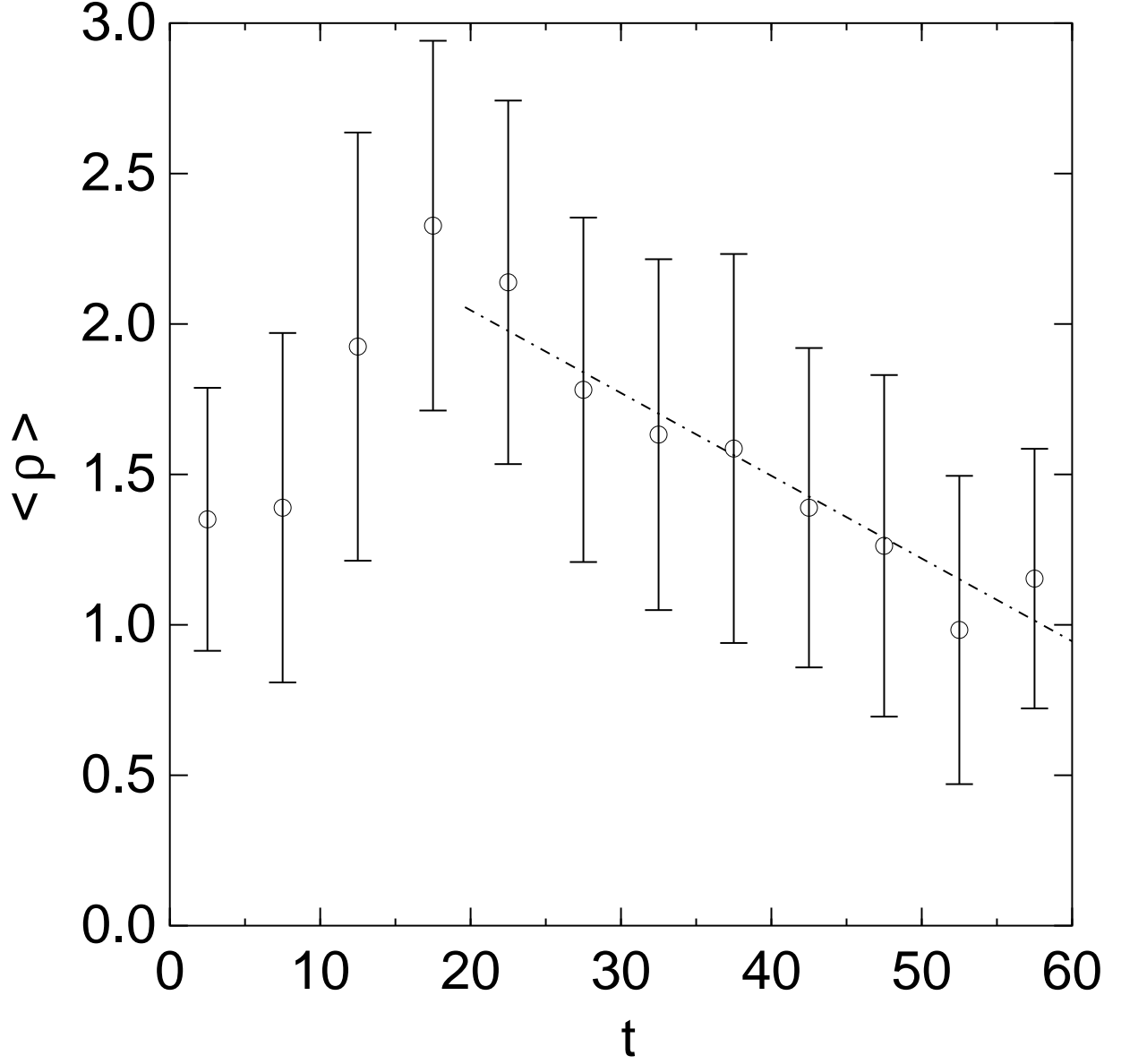


Fig. 10.— Evolution of the stellar density in a central sphere of the cluster with  $r_{\text{csp}} = 0.032$ .  $\rho$  is the average over all simulations, the error-bars represent the standard deviation in the data. The dot-dashed line shows our linear fit for the evolution between 20 and 60 time-units.

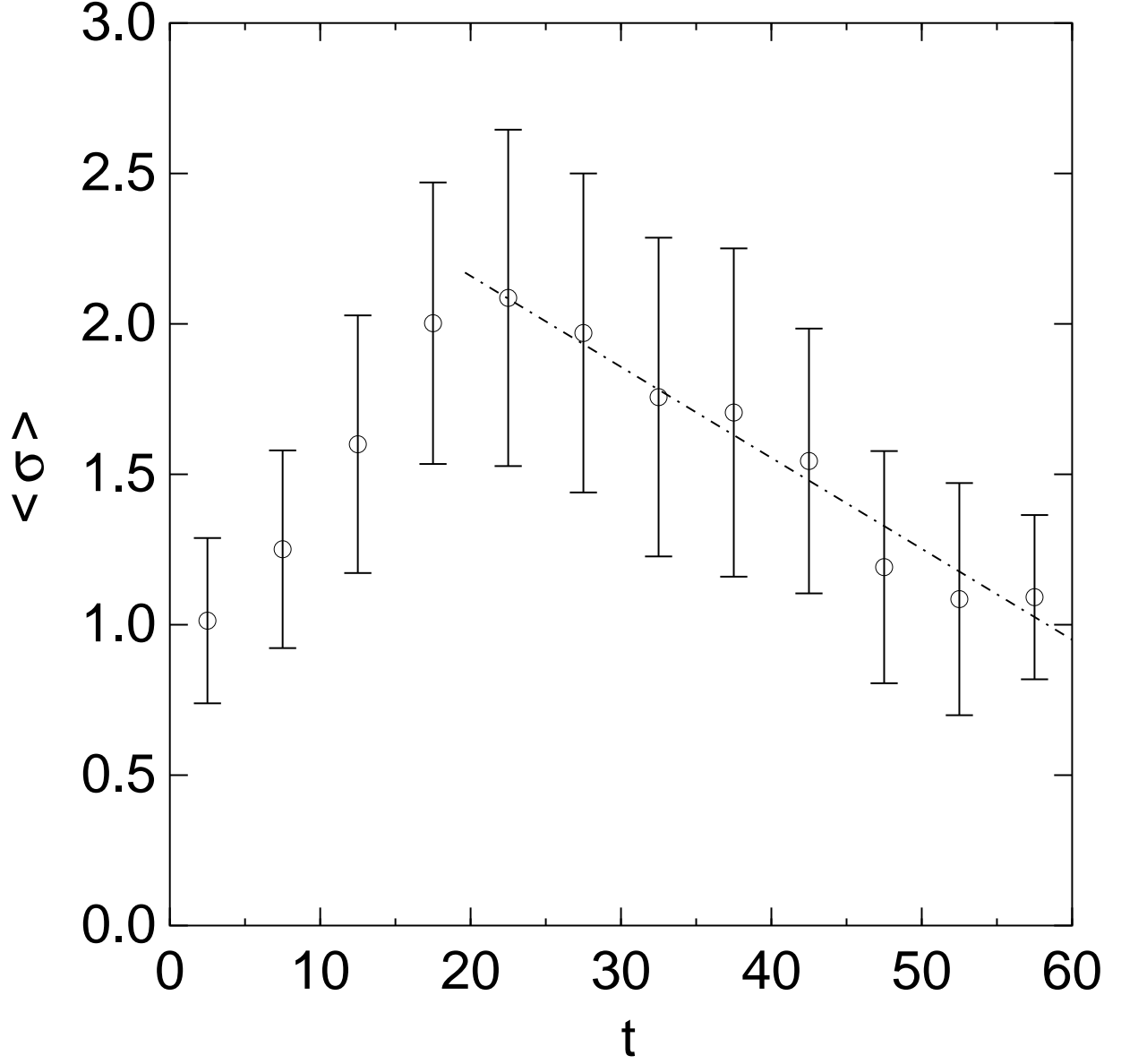


Fig. 11.— Evolution of the stellar velocity dispersion in a central sphere of the cluster with  $r_{\text{csp}} = 0.032$ . The quantity  $\sigma$  is the average from all simulations, the error-bars show the standard deviation in the data. The dot-dashed line shows our linear fit for the evolution between 20 and 60 time-units.

## 6.2. Brownian motion

If the black holes reach equipartition with the stars, their expected mean square velocity follows equation (14). Since our setup involves a Plummer model, we are assuming the binary to move in a harmonic potential in later stages of the simulation. For this reason we expect the motion to follow  $\langle r_{\text{com}}^2 \rangle \propto \langle v_{\text{com}}^2 \rangle$ .

$$\langle v_{\text{equ}}^2 \rangle = \frac{m_*}{m_{\text{com}}} \langle v_*^2 \rangle. \quad (14)$$

While the individual black holes do not reach equipartition, equation (14) can describe the Brownian motion of the system. The sum of the masses is represented by  $m_{\text{com}}$ , the center of mass motion of the binary by  $v_{\text{com}}$ . The mass relation between the stars and the black hole is  $1.53 \cdot 10^{-3}$ ,  $7.63 \cdot 10^{-4}$ , and  $3.81 \cdot 10^{-4}$  in our runs with 32768, 65536, and 131072 particles respectively. However, equation (14) does not describe the behavior of the center of mass motion correctly. While the velocity dispersion drops after 20 time-units  $\langle v_{\bullet}^2 \rangle$  increases. For this reason we compare the measured average  $\langle v_{\text{com}}^2 \rangle$  for the individual particle groups with the mean expectation from the right side of equation (14). For  $\langle v_*^2 \rangle$  we take the average over all simulations neglecting the variability over time. Using this we can estimate  $\langle v_{\text{equ}}^2 \rangle$  and compare it with the measured  $\langle v_{\text{com}}^2 \rangle$ :

$N_{\text{tot}}$	$\langle v_{\text{equ}}^2 \rangle$	$\langle v_{\text{com}}^2 \rangle$	$\langle v_{\text{com}}^2 \rangle / \langle v_{\text{equ}}^2 \rangle$
32768	0.0072	0.0023	3.13
65536	0.0026	0.0011	2.3
131072	0.0022	0.0006	3.9

This means we are finding a center of mass motion for the binary which exceeds the expectations from Brownian motion. However the motion is enhanced by larger factors than proposed by Merritt (2000b). A more detailed discussion on this remains for future work.

## 6.3. Dynamical friction

Following Begelman et al. (1980) dynamical friction becomes inefficient for the binary after it becomes hard. In order to put constraints on this, we try to estimate the influence of dynamical friction on the decay of the binary in the simulation. From Binney and Tremaine (1987) we take the following expression, which is derived from Chandrasekhar (1943).

$$\frac{d\mathbf{v}_{\bullet}}{dt} = -16\pi^2 G^2 \log(\Lambda) M_*(M_{\bullet} + M_*) \frac{\int_0^{v_{\bullet}} v_*^2 f(v_*, \mathbf{r}) dv_*}{v_{\bullet}^3} \mathbf{v}_{\bullet}. \quad (15)$$

Equation (15) describes the deceleration of a particle with mass  $M_\bullet$  under the influence of weak encounters with the surrounding particles with a uniform mass  $M_*$ . In the special case of a Plummer model the integral in equation (15) can be expressed in terms of the escape velocity  $v_{\text{esc}}$  with  $q = v/v_{\text{esc}}$  (Aarseth et al. 1974):

$$\int_0^{v_\bullet} v_*^2 f(v_*, \mathbf{r}) dv_* = \frac{n(\mathbf{r})}{C} \int_0^{q_\bullet} q^2 (1 - q^2)^{\frac{7}{2}} dq, \quad (16)$$

with:

$$C = \int_0^1 q^2 (1 - q^2)^{\frac{7}{2}} dq. \quad (17)$$

The quantity  $n(\mathbf{r})$  defines the number density of the stars at the position  $\mathbf{r}$ . By taking the limit of a gaseous system with  $M_* \ll M_\bullet$ , the term  $n(\mathbf{r})M_*(M_\bullet + M_*)$  becomes  $M_\bullet \rho(\mathbf{r})$ . The integral over  $q$  in equation (16) can be solved in a closed form.

If the motion of the black holes is determined by their self interaction plus a frictional force term, this friction can be linked to the decay of the angular momentum  $l$  as follows:

$$\mathbf{a} = \mathbf{a}_r + a_{\text{df}} \frac{\mathbf{v}}{v}, \quad (18)$$

$$\dot{l} = \frac{ma_{\text{df}}}{v} (\mathbf{r} \times \mathbf{v}) = \frac{la_{\text{df}}}{v}. \quad (19)$$

With equation (15) and (16) we can evaluate the dynamical friction (19) according to:

$$\frac{\dot{l}}{l} = -\frac{16\pi^2 G^2}{C v_\bullet^3} \log(\Lambda) M_\bullet \rho(\mathbf{r}) \int_0^{q_\bullet} q^2 (1 - q^2)^{\frac{7}{2}} dq \quad (20)$$

The gravitational constant  $G$  is unity in our model units and the black holes have the mass  $M_\bullet = 0.01$  each. We use the mean orbital velocities for  $v_\bullet$ . In order to evaluate  $\rho(r)$  we use the mean distance of the black holes for  $r$  which introduces only a very small error in a Plummer model. Assuming a linear behavior for  $\lg(l) = a + bt$  we find  $\dot{l}/l = b \ln(10)$ . We can use this to estimate the angular momentum from the slopes  $b$  of the linear fits in figure 9. As result we find  $\log(\Lambda) \approx 0.15$  and being constant within the error margins. This result shows that the usual assumption for  $\Lambda$  being large does not hold.

## 7. Physical units

As stated before, the collisional simulations which include very massive particles do not reach the observed mass contrast in galactic nuclei. All simulations are carried out by using



model units. In order to transform these units to physical units a system size in parsec or a stellar mass in units of solar masses has to be chosen. With the knowledge of the gravitational constant  $G$  all remaining units can be rescaled (Heggie and Mathieu 1986).

In the following a run with 65536 particles is scaled to a physical stellar system. Since this work focuses on the dynamics of galactic nuclei, the physical mass of the supermassive objects motivates the following choices:

$$M_{\bullet} := 1.00015 \cdot 10^7 M_{\odot}, \quad (21)$$

$$M_{*} := 1.49536 \cdot 10^4 M_{\odot}. \quad (22)$$

The masses are chosen so that the total mass of the system is  $M_{\text{tot}} = 10^9 M_{\odot}$  and the mean mass of a particle is  $\bar{M} = 1.52588 \cdot 10^4 M_{\odot}$ . This choice means that every stellar particle with mass  $M_{*}$  represents a compact star cluster with the order of  $10^4$  particles. The chosen mass for the black hole particle has approximately the same mass as the central black hole of M31 (Magorrian et al. 1998).

The conversion between physical units and  $N$ -body units follows  $x_{\text{phys}} = X_{\text{conv}} x_{\text{sim}}$  for simulated quantities. By choosing the central velocity dispersion to be 110 km/s, we find  $T_{\text{conv}}$  and  $R_{\text{conv}}$ :

$$R_{\text{conv}} = 355.39 \text{ pc}, \quad (23)$$

$$M_{\text{conv}} = 10^9 M_{\odot}, \quad (24)$$

$$T_{\text{conv}} = 3.1590 \cdot 10^6 \text{ y}, \quad (25)$$

$$V_{\text{conv}} = 110 \text{ km/s}. \quad (26)$$

In a Plummer model the half mass radius  $r_h$  is connected with the Plummer radius  $R$  by  $r_h = 1.30R$  (Spitzer 1987). Since  $R = 3\pi/16$  the half mass radius is in model units at  $r_h = 0.766$ . Therefore, the initial model for the simulated decay of a black hole in the galactic center is a Plummer sphere with a half mass radius of 272.23 pc. The initial distance between the black holes is 355.39 pc. They become bound after approximately 40 million years. The total simulated time is approximately 190 million years. At the end of the simulation the black holes' distance varies between 1 pc at the apo-center and 0.2 pc at the peri-center. The semi-major axis of the first bound orbit is 21 pc.

## 8. Conclusions

We have created a new  $N$ -body hybrid code merging a high accuracy direct Hermite integrator of the standard type (Aarseth 1999; Spurzem and Kugel 1999) with a collisionless

$N$ -body method, approximating the potential of a given particle distribution by a series expansion, generally known as “SCF” (Hernquist and Ostriker 1992; Zhao 1996). The SCF method has been completely rewritten to include a computation of the time derivative of the gravitational force and a fourth order Hermite integrator. We use this code to model a galactic nucleus containing two massive black holes with up to 128k single particles. The evolution of the binary black hole is followed from an initial phase, driven by standard dynamical friction to a phase where the binary is bound and further hardened by three-body encounters with single stars. In that hardening phase we take full advantage of the regularized three-body integration developed by Mikkola and Aarseth (1996) and Mikkola and Aarseth (1998). The method proves to work well, and reproduces standard expectations such as the Chandrasekhar dynamical friction in the initial phase. In the final hardening phase due to three body encounters we find, that the eccentricity of the black hole binary remains at a fairly large value (around 0.7), which is very interesting because it decreases the time scale for gravitational radiation merger of binary black holes dramatically, and thus increases our chances to detect gravitational radiation from such events via LISA. Due to computational limitations, however, our particle numbers are still not large enough to describe the real physical situation. Any scaling is problematic and so further work with improved hardware and software should be done.

We study in detail the motion of the black hole binary in the center of a galaxy. It turns out that it does not decay as expected with increasing particle number. The mechanism exciting these motions is yet unclear. If they exist up to realistic particle numbers they will solve the problem of feeding the black holes with fresh stellar dynamical material, which was raised by Gould and Rix (2000).

## 9. Acknowledgements

The authors would like to thank S. Aarseth, D. Heggie, W. Sweatman, C. Theis, C. Boily, D. Merritt, M. Milosavljević, F. Cruz, H. Baumgardt, G. Hensler, L. Hernquist and H. S. Zhao for fruitful help and discussion. This project is funded by *Deutsche Forschungsgemeinschaft* (DFG) project Sp 345/9-1,2 and Sonderforschungsbereich (SFB) 439 funded at the University of Heidelberg, NSF grant AST 00-71099, NASA grants NAG 5-7019, NAG 5-6037, and NAG 5-9046. Technical help and computer resources are provided by *NIC* in Jülich, *HLRS* in Stuttgart, *TRACS* and *EPCC* in Edinburgh, *ZIB* in Berlin, *SSC* in Karlsruhe, University of Heidelberg, Rutgers University, and University of Kiel, and by the Pittsburgh Supercomputer Center and the San Diego Supercomputer Center. The authors thank the Aspen Center for Physics, the Institute of Astronomy and the Lorenz center at

Leiden University for hospitality. The sources for EuroStar are available from the authors or via <http://www.physics.rutgers.edu/~marchems/>

## REFERENCES

- Aarseth, S. 1996, in P. Hut and J. Makino (eds.), *Dynamical Evolution of Star Clusters*, pp 161–170, International Astronomical Union
- Aarseth, S. J. 1993, in G. Contopoulos, N. K. Spyrou, and L. Vlahos (eds.), *Galactic Dynamics and N-body Simulations*, Vol. 433 of *Lecture Notes in Physics*, pp 365–417, Springer–Verlag, Thessaloniki
- Aarseth, S.J. 1999, *Celest. Mech. Dyn. Astron.* **73**, 127
- Aarseth, S.J., Hénon, M., Wielen, R. 1974, *A&A* **37**, 183
- Abramowitz, M. and Stegun, I. A. (eds.) 1972, *Handbook of mathematical functions*, Dover, New York, 9. edition
- Ahmad, A. and Cohen, L. 1973, *Journal of Computational Physics* **12**, 349
- Begelman, M. C., Blandford, R. D., and Rees, M. J. 1980, *Nature* **287**, 307
- Binney, J. and Tremaine, S. 1987, *Galactic Dynamics*, Princeton University Press, Princeton, 1. edition
- Boccaletti, D. and Pucacco, G. 1996, *Theory of Orbits*, Vol. 1 of *Astronomy and Astrophysics Library*, Springer Verlag, Berlin, Heidelberg, New York, 1. edition
- Chandrasekhar, S. 1943, *ApJ* **97**, 255
- Clutton-Brock, M. 1973, *Astrophysics and Space Science* **23**, 55
- Danzmann, K. 2000, *Fundamental Physics in Space*, Proceedings of the H0.1 Symposium of COSPAR Scientific Commission H, held during the 32nd COSPAR Scientific Assembly, ed. S. Vitale, Pergamon Press, p. 1129
- Diaferio, A., Kauffmann, G., Colberg, J.M., White, S.D.M. 1999, *MNRAS* **307**, 537
- Ferrarese, L., Merritt, D. 2000, *ApJ* **539**, L9

- Gebhardt, K., Bender, R., Bower, G., Dressler, A., Faber, S.M., Filippenko, A.V., Green, R., Grillmair, Carl, Ho, L.C., Kormendy, J., Lauer, T.R., Magorrian, J., Pinkney, J., Richstone, D., Tremaine, S. 2000, *ApJ* **539**, L13
- Gould, A. and Rix, H.-W. 2000, *ApJ* **532**, L29
- Haehnelt, M.G., Kauffmann, G. 2000, *MNRAS* **318**, L35
- Halpern, J.P., Eracleous, M. 2000, *ApJ* **531**, 647
- Heggie, D. C. and Mathieu, R. M. 1986, in P. Hut and S. L. W. McMillan (eds.), *The use of supercomputers in stellar dynamics*, pp 233–235, New York
- Hernquist, L. and Ostriker, J. P. 1992, *ApJ* **386**, 375
- Hernquist, L., Sigurdsson, S. and Bryan, G. L. 1995, *ApJ* **446**, 717
- Hills, J. G. 1992, *AJ* **103**, 1955
- Holley-Bockelmann, K., Mihos, J.C., Sigurdsson, S. and Hernquist, L. 2001 *ApJ*, in press
- Kauffmann, G., Colberg, J.M., Diaferio, A., White, S.D.M. 1999a, *MNRAS* **307**, 529
- Kauffmann, G., Colberg, J.M., Diaferio, A., White, S.D.M. 1999b, *MNRAS* **303**, 188
- Kauffmann, G., Haehnelt, M.G. 2000, *MNRAS* **311**, 576
- Kormendy, J. and Richstone, D. 1995, *ARA&A* **33**, 581
- Kustaanheimo, P. and Stiefel, E. 1965, *Journal für die reine und angewandte Mathematik* **218**, 204
- Lehto, H.J., Valtonen, M.J. 1996, *ApJ* **460**, 207
- Magorrian, J., Tremaine, S., Richstone, D., Bender, R., Bower, G., Dressler, A., Faber, S. M., Gebhardt, K., Green, R., Grillmayr, C., Kormendy, J., and Lauer, T. 1998, *AJ* **115**, 2285
- Makino, J. 1997, *ApJ* **478**, 58
- Makino, J., Fukushige, T., Okumura, S. K., and Ebisuzaki, T. 1993, *PASJ* **45**, 303
- Merritt, D. 2000a, in F. Combes (ed.), *Galaxies and the universe*, ASP-Conference series, pp 221–, Paris

- Merritt, D. 2000b, *Brownian motion of a massive binary*, astro-ph/0012264
- Merritt, D. and Ferrarese, L. 2001, *MNRAS* **320**, L30
- Merritt, D. and Quinlan, G. D. 1998, *ApJ* **498**, 625
- Mikkola S., Aarseth S.J. 1996, *Cel. Mech. Dyn. Astron.* **64** 197
- Mikkola S., Aarseth S.J. 1998, *NewA* **3**, 309
- Mikkola, S. and Valtonen, M. J. 1992, *MNRAS* **259**, 115
- Navarro, J.F., Steinmetz, M. 2000, *ApJ* **538**, 477
- Peebles, P. J. E. 1993, *Principles of physical cosmology*, Princeton University Press, Princeton, 1. edition
- Phinney, E.S. 2000, *American Astronomical Society, HEAD meeting* **32**, 46.01
- Quinlan, G. D. 1996, *NewA* **1**, 35
- Quinlan, G. D. and Hernquist, L. 1997, *NewA* **2**, 533
- Richstone, D., Ajhar, E.A., Bender, R., Bower, G., Dressler, A., Faber, S.M., Filippenko, A.V., Gebhardt, K., Green, R., Ho, L.C., Kormendy, J., Lauer, T.R., Magorrian, J., Tremaine, S. 1998, *Nature* **395**, 14
- Sigurdsson, S., He, B., Melhem, R. and Hernquist, L. 1997 *Computers in Physics* **11.4**, 378
- Spitzer, L. J. 1987, *Dynamical evolution of globular clusters*, Princeton University Press, Princeton, NJ, 1. edition
- Spurzem, R. 1999, *The Journal of Computational and Applied Mathematics* **109**, 407
- Spurzem, R. and Baumgardt, H. 2001, *A parallel implementation of an Aarseth N-body integrator on general and special purpose supercomputers*, ARI-Preprint No. 68, submitted to MNRAS
- Spurzem, R. and Kugel, A. 1999, *Towards the million body problem on the computer – no news since the three-body-problem?*, astro-ph/9906155, to appear in Procs. of Molecular Dynamics on Parallel Computers, Workshop of the John von Neumann-Institute for Computing (NIC) Jülich, 1999, World Scientific, Singapore

- Sugimoto, D., Makino, J., Taiji, M., and Ebisuzaki, T. 1995, in *Proceedings of the first Aizu international symposium on parallel algorithms / architecture synthesis*, pp 38–44, IEEE Computer Society
- Valtonen, M. J., Mikkola, S., Heinämäki, P., and Valtonen, H. 1994, *ApJS* **95**, 69
- Zhao, H. 1996, *MNRAS* **278**, 488

### A. Recurrence relations for Ultraspherical polynomials

Throughout the computation for the forces and force derivatives in our SCF-scheme several special functions have to be tabulated. Recurrence relations provide a very efficient way for that. The following recursion relations have been applied to compute ultraspherical polynomials and their derivatives. As starting values for  $n \in 0, 1$  the recurrence formulae for the Gegenbauer or ultraspherical polynomials obey:

$$C_n^{(\alpha)}(\xi) = \begin{cases} 1 & \text{if } n = 0, \\ 2\alpha\xi & \text{if } n = 1. \end{cases} \quad (\text{A1})$$

The expressions for higher values are given by:

$$C_{n+1}^{(\alpha)}(\xi) = \frac{2(n + \alpha)\xi C_n^{(\alpha)}(\xi) - (n + 2\alpha - 1)C_{n-1}^{(\alpha)}(\xi)}{(n + 1)} \quad (\text{A2})$$

From that the first derivative can be computed as: (Abramowitz and Stegun (1972), equation (22.7.22) and table 22.7.)

$$C_{n-1}^{(\alpha+1)}(\xi) = \frac{(n + 2\alpha)\xi C_n^{(\alpha)}(\xi) - (n + 1)C_{n+1}^{(\alpha)}(\xi)}{2\alpha(1 - \xi^2)} \quad (\text{A3})$$

For practical reasons and higher accuracy the second derivative polynomial is computed using equation (A2):

$$C_{n+1}^{(\alpha+2)}(\xi) = \frac{2(n + \alpha + 2)\xi C_n^{(\alpha+2)}(\xi) - (n + 2(\alpha + 2) - 1)C_{n-1}^{(\alpha+2)}(\xi)}{(n + 1)} \quad (\text{A4})$$

Because the particle track is approximated by using the Hermite scheme, one has to find forces and the first force derivative in one go. An approximation using two timesteps for the first force derivative introduces errors to the second and third derivative of the forces. All particles move within a time dependent potential; therefore, the first derivative has a term describing the change of the potential and a term describing the change of force depending on the particle's orbit.

$$\frac{d}{dt} \mathbf{a}(t, \mathbf{r}) = \frac{\partial \mathbf{a}(t, \mathbf{r})}{\partial t} + \frac{\partial \mathbf{r}}{\partial t} \frac{\partial \mathbf{a}(t, \mathbf{r})}{\partial \mathbf{r}}. \quad (\text{A5})$$

With the help of the orbit integration for the single particle in a given static potential case, equation (A5) evaluates to:

$$\begin{aligned} \frac{d}{dt} \mathbf{a}(t, \mathbf{r}) = & \left( \frac{\partial a_r}{\partial t} + \frac{\partial a_r}{\partial r} \dot{r} + \frac{\partial a_r}{\partial \vartheta} \dot{\vartheta} + \frac{\partial a_r}{\partial \varphi} \dot{\varphi} - a_{\vartheta} \dot{\vartheta} - a_{\varphi} \dot{\varphi} \sin \vartheta \right) \mathbf{e}_r \\ & + \left( \frac{\partial a_{\vartheta}}{\partial t} + \frac{\partial a_{\vartheta}}{\partial r} \dot{r} + \frac{\partial a_{\vartheta}}{\partial \vartheta} \dot{\vartheta} + \frac{\partial a_{\vartheta}}{\partial \varphi} \dot{\varphi} + a_r \dot{\vartheta} - a_{\varphi} \dot{\varphi} \cos \vartheta \right) \mathbf{e}_{\vartheta} \\ & + \left( \frac{\partial a_{\varphi}}{\partial t} + \frac{\partial a_{\varphi}}{\partial r} \dot{r} + \frac{\partial a_{\varphi}}{\partial \vartheta} \dot{\vartheta} + \frac{\partial a_{\varphi}}{\partial \varphi} \dot{\varphi} + a_r \dot{\varphi} \sin \vartheta + a_{\vartheta} \dot{\varphi} \cos \vartheta \right) \mathbf{e}_{\varphi} \end{aligned} \quad (\text{A6})$$

The evaluation of the first term on the right hand side of equation (A5) is given in section B. The derivatives with respect to the spatial coordinates in equation (A6) can be found in section C.

## B. Time-dependency of the potential

Because all positions and velocities of the dataset are time-dependent, the partial derivatives with respect to  $t$  apply only to the coefficients  $A_{nlm}$ . These are implemented as the variables  $C_{lm}(r)$ ,  $D_{lm}(r)$ ,  $E_{lm}(r)$ , and  $F_{lm}(r)$ , from which the partial derivative can be formed:

$$\frac{\partial C_{lm}(r)}{\partial t} = N_{lm} \sum_{n=0}^{\infty} \tilde{A}_{nl} \tilde{\Phi}_{nl}(r) \sum_k m_k \frac{\partial}{\partial t} \left( \tilde{\Phi}_{nl}(r_k) P_{lm}(\cos(\vartheta_k)) \cos(m\varphi_k) \right), \quad (\text{B1})$$

$$\frac{\partial D_{lm}(r)}{\partial t} = N_{lm} \sum_{n=0}^{\infty} \tilde{A}_{nl} \tilde{\Phi}_{nl}(r) \sum_k m_k \frac{\partial}{\partial t} \left( \tilde{\Phi}_{nl}(r_k) P_{lm}(\cos(\vartheta_k)) \sin(m\varphi_k) \right), \quad (\text{B2})$$

$$\frac{\partial E_{lm}(r)}{\partial t} = N_{lm} \sum_{n=0}^{\infty} \tilde{A}_{nl} \frac{d\tilde{\Phi}_{nl}(r)}{dr} \sum_k m_k \frac{\partial}{\partial t} \left( \tilde{\Phi}_{nl}(r_k) P_{lm}(\cos(\vartheta_k)) \cos(m\varphi_k) \right), \quad (\text{B3})$$

$$\frac{\partial F_{lm}(r)}{\partial t} = N_{lm} \sum_{n=0}^{\infty} \tilde{A}_{nl} \frac{d\tilde{\Phi}_{nl}(r)}{dr} \sum_k m_k \frac{\partial}{\partial t} \left( \tilde{\Phi}_{nl}(r_k) P_{lm}(\cos(\vartheta_k)) \sin(m\varphi_k) \right). \quad (\text{B4})$$

With:

$$\frac{\partial}{\partial t} \tilde{\Phi}_{nl}(r_k) = \frac{\partial r_k}{\partial t} \tilde{\Phi}_{nl}(r_k) + \left[ \frac{l}{r_k} - \frac{r_k^{\frac{1}{\alpha}}}{r_k} \frac{2l+1}{1+r_k^{\frac{1}{\alpha}}} + \frac{4r_k^{\frac{1}{\alpha}}}{r_k} \frac{\alpha(2l+1) + \frac{1}{2}}{\alpha(1+r_k^{\frac{1}{\alpha}})^2} \frac{C_{n-1}^{(\omega+1)}(\xi_k)}{C_n^{(\omega)}(\xi_k)} \right], \quad (\text{B5})$$

$$\frac{\partial}{\partial t} P_{lm}(\cos(\vartheta_k)) = -\frac{\partial \vartheta_k}{\partial t} \sin(\vartheta_k) \frac{\partial P_{lm}(\cos(\vartheta_k))}{\partial \cos(\vartheta_k)}, \quad (\text{B6})$$

$$\frac{\partial}{\partial t} \cos(m\varphi_k) = -m \frac{\partial \varphi_k}{\partial t} \sin(m\varphi_k), \quad (\text{B7})$$

$$\frac{\partial}{\partial t} \sin(m\varphi_k) = m \frac{\partial \varphi_k}{\partial t} \cos(m\varphi_k). \quad (\text{B8})$$

in the coefficient computation section the standard leap frog integrator provided by Hernquist and Ostriker (1992) is extended by two additional variables, which are computed by using the recursion relations in section A.

### C. Orbit dependency of the force derivative

In order to account for the change of force due to the particle orbit one has to calculate the nine partial derivatives in equation (A6). These nine derivatives will now be listed. In order to save some space the second derivative of  $\tilde{\Phi}_{nl}(r)$  is given first:

$$\begin{aligned} \frac{\partial^2}{\partial r^2} \tilde{\Phi}_{nl}(r) = & \tilde{\Phi}_{nl}(r) \left[ \left( \frac{l}{r} - \frac{r^{\frac{1}{\alpha}}}{r} \frac{(2l+1)}{(1+r^{\frac{1}{\alpha}})} \right)^2 - \frac{l}{r^2} \right. \\ & + \frac{(2l+1)}{(1+r^{\frac{1}{\alpha}})^2} \frac{r^{\frac{1}{\alpha}}}{\alpha r^2} (\alpha - 1 + \alpha r^{\frac{1}{\alpha}}) \\ & + \left[ 8 \left( \frac{r^{\frac{1}{\alpha}}}{r} \frac{\omega}{\alpha(1+r^{\frac{1}{\alpha}})^2} \right) \left( \frac{l}{r} - \frac{r^{\frac{1}{\alpha}}}{r} \frac{(2l+1)}{(1+r^{\frac{1}{\alpha}})} \right) \right. \\ & + \left. \left. \frac{4\omega r^{\frac{1}{\alpha}}}{r^2 \alpha^2 (1+r^{\frac{1}{\alpha}})^3} (1 - \alpha - (\alpha+1)r^{\frac{1}{\alpha}}) \right] \frac{C_{n-1}^{(\omega+1)}(\xi)}{C_n^{(\omega)}(\xi)} \right. \\ & + 16 \left( \frac{r^{\frac{1}{\alpha}}}{\alpha r} \right)^2 \frac{\omega(\omega+1)}{(1+r^{\frac{1}{\alpha}})^4} \frac{C_{n-2}^{(\omega+2)}(\xi)}{C_n^{(\omega)}(\xi)} \end{aligned} \quad (\text{C1})$$

The nine derivatives can be implemented as follows:



### C.1. Derivatives with respect to $r$

The radial derivative for the radial acceleration becomes:

$$\frac{\partial a_r}{\partial r} = - \sum_{l=0}^{\infty} \sum_{m=0}^{\infty} P_{lm}(\cos(\vartheta)) [G_{lm}(r) \cos(m\varphi) + H_{lm}(r) \sin(m\varphi)], \quad (\text{C2})$$

with:

$$G_{lm} = N_{lm} \sum_{n=0}^{\infty} \tilde{A}_{nl} \frac{\partial^2}{\partial r^2} \tilde{\Phi}_{nl}(r) \sum_k m_k \tilde{\Phi}_{nl}(r_k) P_{lm}(\cos(\vartheta_k)) \cos(m\varphi_k), \quad (\text{C3})$$

$$H_{lm} = N_{lm} \sum_{n=0}^{\infty} \tilde{A}_{nl} \frac{\partial^2}{\partial r^2} \tilde{\Phi}_{nl}(r) \sum_k m_k \tilde{\Phi}_{nl}(r_k) P_{lm}(\cos(\vartheta_k)) \sin(m\varphi_k). \quad (\text{C4})$$

The radial derivative for the acceleration in  $\vartheta$  direction becomes:

$$\begin{aligned} \frac{\partial a_{\vartheta}}{\partial r} = & - \sin(\vartheta) \sum_{l=0}^{\infty} \sum_{m=0}^{\infty} \frac{\partial P_{lm}(\cos(\vartheta))}{\partial \cos(\vartheta)} \\ & \left[ \left( \frac{1}{r^2} C_{lm}(r) - \frac{1}{r} E_{lm}(r) \right) \cos(m\varphi) + \right. \\ & \left. \left( \frac{1}{r^2} D_{lm}(r) - \frac{1}{r} F_{lm}(r) \right) \sin(m\varphi) \right]. \end{aligned} \quad (\text{C5})$$

The radial derivative for the acceleration in  $\varphi$  direction becomes:

$$\begin{aligned} \frac{\partial a_{\varphi}}{\partial r} = & \sum_{l=0}^{\infty} \sum_{m=0}^{\infty} \frac{m P_{lm}(\cos(\vartheta))}{\sin(\vartheta)} \\ & \left[ \left( \frac{1}{r^2} D_{lm}(r) - \frac{1}{r} F_{lm}(r) \right) \cos(m\varphi) - \right. \\ & \left. \left( \frac{1}{r^2} C_{lm}(r) - \frac{1}{r} E_{lm}(r) \right) \sin(m\varphi) \right]. \end{aligned} \quad (\text{C6})$$

### C.2. Derivatives with respect to $\vartheta$

The derivative with respect to  $\vartheta$  for the radial acceleration becomes:

$$\frac{\partial a_r}{\partial \vartheta} = \sin(\vartheta) \sum_{l=0}^{\infty} \sum_{m=0}^{\infty} \frac{\partial P_{lm}(\cos(\vartheta))}{\partial \cos(\vartheta)} [E_{lm}(r) \cos(m\varphi) + F_{lm}(r) \sin(m\varphi)]. \quad (\text{C7})$$

The derivative with respect to  $\vartheta$  for the acceleration in  $\vartheta$  direction becomes:

$$\begin{aligned} \frac{\partial a_\vartheta}{\partial \vartheta} = \frac{1}{r} \sum_{l=0}^{\infty} \sum_{m=0}^{\infty} \left( \cos(\vartheta) \frac{\partial P_{lm}(\cos(\vartheta))}{\partial \cos(\vartheta)} - \sin^2(\vartheta) \frac{\partial^2 P_{lm}(\cos(\vartheta))}{\partial \cos(\vartheta)^2} \right) \\ [C_{lm}(r) \cos(m\varphi) + D_{lm}(r) \sin(m\varphi)]. \end{aligned} \quad (\text{C8})$$

The derivative with respect to  $\vartheta$  for the acceleration in  $\varphi$  direction becomes:

$$\begin{aligned} \frac{\partial a_\varphi}{\partial \vartheta} = \frac{1}{r} \sum_{l=0}^{\infty} \sum_{m=0}^{\infty} m \left( \frac{\partial P_{lm}(\cos(\vartheta))}{\partial \cos(\vartheta)} + \cos(\vartheta) \frac{P_{lm}(\cos(\vartheta))}{\sin^2(\vartheta)} \right) \\ [D_{lm}(r) \cos(m\varphi) - C_{lm}(r) \sin(m\varphi)]. \end{aligned} \quad (\text{C9})$$

### C.3. Derivatives with respect to $\varphi$

The derivative with respect to  $\varphi$  for the acceleration in radial direction becomes:

$$\frac{\partial a_r}{\partial \varphi} = - \sum_{l=0}^{\infty} \sum_{m=0}^{\infty} m P_{lm}(\cos(\vartheta)) [F_{lm}(r) \cos(m\varphi) - E_{lm}(r) \sin(m\varphi)]. \quad (\text{C10})$$

The derivative with respect to  $\varphi$  for the acceleration in  $\vartheta$  direction becomes:

$$\frac{\partial a_\vartheta}{\partial \varphi} = \frac{\sin(\vartheta)}{r} \sum_{l=0}^{\infty} \sum_{m=0}^{\infty} m \frac{\partial P_{lm}(\cos(\vartheta))}{\partial \cos(\vartheta)} [D_{lm}(r) \cos(m\varphi) - C_{lm}(r) \sin(m\varphi)]. \quad (\text{C11})$$

The derivative with respect to  $\varphi$  for the acceleration in  $\varphi$  direction becomes:

$$\frac{\partial a_\varphi}{\partial \varphi} = \frac{1}{r} \sum_{l=0}^{\infty} \sum_{m=0}^{\infty} m^2 \frac{P_{lm}(\cos(\vartheta))}{\sin(\vartheta)} [C_{lm}(r) \cos(m\varphi) + D_{lm}(r) \sin(m\varphi)]. \quad (\text{C12})$$

$\langle t \rangle_{\text{bin}}$	32768	65536	131072	all runs
2.5	2501	1000	2192	5693
7.5	2505	1508	3621	7634
12.5	2681	4487	24536	31704
17.5	3264	5581	32814	41659
22.5	11987	6709	90249	108945
27.5	3630	5528	7383	16541
32.5	5766	2255	7568	15589
37.5	4984	5541	254	10779
47.5	1783	7447	–	10342
42.5	7768	2574	–	9230
52.5	1440	637	–	2077
57.5	1045	4567	–	5612
total	49354	47834	168617	265805

Table 1: Number of sample points in the bins used for analyzing the motion of the binary. The bin for the evolution time  $t$  in  $N$ -body units are centered around  $\langle t \rangle_{\text{bin}}$ . Plots using bins for the total particle number  $N_{\text{tot}}$  have the number of sample points given in the row labeled “total”.